OPEN ACCESS
CellPress

Cell Reports
Report

Aberrant Active *cis*-Regulatory Elements Associated with Downregulation of RET Finger Protein Overcome Chemoresistance in Glioblastoma

Melissa Ranjit,[1,8] Masaki Hirano,[1,8] Kosuke Aoki,[1] Yusuke Okuno,[2] Fumiharu Ohka,[1] Akane Yamamichi,[1] Akira Kato,[1] Sachi Maeda,[1] Kazuya Motomura,[1] Keitaro Matsuo,[3,4] Atsushi Enomoto,[5] Yasushi Ino,[6] Tomoki Todo,[6] Masahide Takahashi,[5] Toshihiko Wakabayashi,[1] Takuya Kato,[7,*] and Atsushi Natsume[1,9,*]

[1]Department of Neurosurgery, Nagoya University School of Medicine, Nagoya, Japan
[2]Center for Advanced Medicine and Clinical Research, Nagoya University Hospital, Nagoya, Japan
[3]Division of Cancer Epidemiology and Prevention, Aichi Cancer Center Research Institute, Nagoya, Japan
[4]Department of Epidemiology, Nagoya University School of Medicine, Nagoya, Japan
[5]Department of Pathology, Nagoya University School of Medicine, Nagoya, Japan
[6]Division of Innovative Cancer Therapy, Advanced Clinical Research Center, Institute of Medical Science, The University of Tokyo, Tokyo, Japan
[7]Department of Pathology, Kitasato University School of Medicine, Sagamihara, Japan
[8]These authors contributed equally
[9]Lead Contact
*Correspondence: katot@med.kitasato-u.ac.jp (T.K.), anatsume@med.nagoya-u.ac.jp (A.N.)
https://doi.org/10.1016/j.celrep.2019.01.109

SUMMARY

RET finger protein (RFP) forms a complex with histone deacetylase 1, resulting in aberrant deacetylation of H3K27ac and dysregulation of *cis*-regulatory elements. We evaluated the modulatory effects of RFP knockdown on *cis*-regulatory elements, gene expression, and chemosensitivity to temozolomide both in glioblastoma cells and in an intracranial glioblastoma model. The combination of RFP knockdown and temozolomide treatment markedly suppressed the glioblastoma cell growth due to oxidative stress and aberrant cell cycle and increased survival time in mice with glioblastoma. ChIP-seq and RNA-seq revealed that RFP knockdown increased or decreased activity of numerous *cis*-regulatory elements that lie adjacent to genes that control functions such as apoptosis, mitosis, DNA replication, and cell cycle: *FOXO1*, *TBP2*, and *PARPBP*. This study suggests that RFP contributes to chemoresistance via aberrant deacetylation of histone H3 at K27, whereas dysregulation of RFP-associated *cis*-regulatory elements in glioma and RFP knockdown combined with temozolomide is an effective treatment strategy for lethal glioma.

INTRODUCTION

The status of histone H3 lysine 27 (H3K27) acetylation (ac) controls active *cis*-regulatory elements that increase gene transcription (Creyghton et al., 2010). Histone deacetylases (HDACs) deacetylate lysine residues on core histones, leading to a decrease in gene transcription (Marks et al., 2003; Mottet and Castronovo, 2008). In *cis*-regulatory-element regions, complexes containing HDAC maintain histones in a repressed state by H3K27ac deacetylation (Heinz et al., 2015).

Glioblastoma (GBM) is the most aggressive brain tumor with a median survival period of only 14.6 months (Stupp et al., 2005). Temozolomide (TMZ) is a mainstream drug but yields a 5-year survival rate of 10% in GBM (Stupp et al., 2005, 2009). TMZ acts by methylating guanine residues, rendering the DNA mismatch repair system (MMR) unable to find a complementary base for that methylated guanine, thereby leading to glioma cell death. O^6-methylguanine DNA methyltransferase (MGMT) demethylates those guanine residues and constitutes a DNA repair system resulting in chemoresistance (Hermisson et al., 2006). PARP1 also contributes to TMZ resistance via the base excision repair (BER) pathway (Tentori et al., 2003). PARP-binding protein (PARPBP) is upregulated in various types of cancer (Piao et al., 2011).

RET finger protein (RFP) or tripartite-motif-containing 27 (TRIM27) is a transcription factor that becomes oncogenic upon fusion with RET tyrosine kinase (Reymond et al., 2001; Takahashi et al., 1988; Hasegawa et al., 1996). RFP is involved in cell growth (Shimono et al., 2000) and apoptosis (McNab et al., 2011), and is expressed in many types of cancer (Tezel et al., 1999; Isomura et al., 1992; Takahashi et al., 1985, 1988; Tsukamoto et al., 2009; Iwakoshi et al., 2012). RFP forms a tripartite complex with HDAC1 and nuclear transcription factor Y (NF-Y). An RFP knockdown (RFP-KD) disrupts the RFP-HDAC1-NF-Y complex, subsequently increasing expression of thioredoxin binding protein-2 (TBP-2) (Kato et al., 2009). This phenomenon has also been found to increase chemosensitivity to cisplatin in cancer cells.

Here, we determined whether RFP-KD causes TMZ chemosensitivity in TMZ-resistant gliomas and whether the disruption of the RFP-HDAC1 complex can disorder active *cis*-regulatory elements that are controlled by H3K27ac.

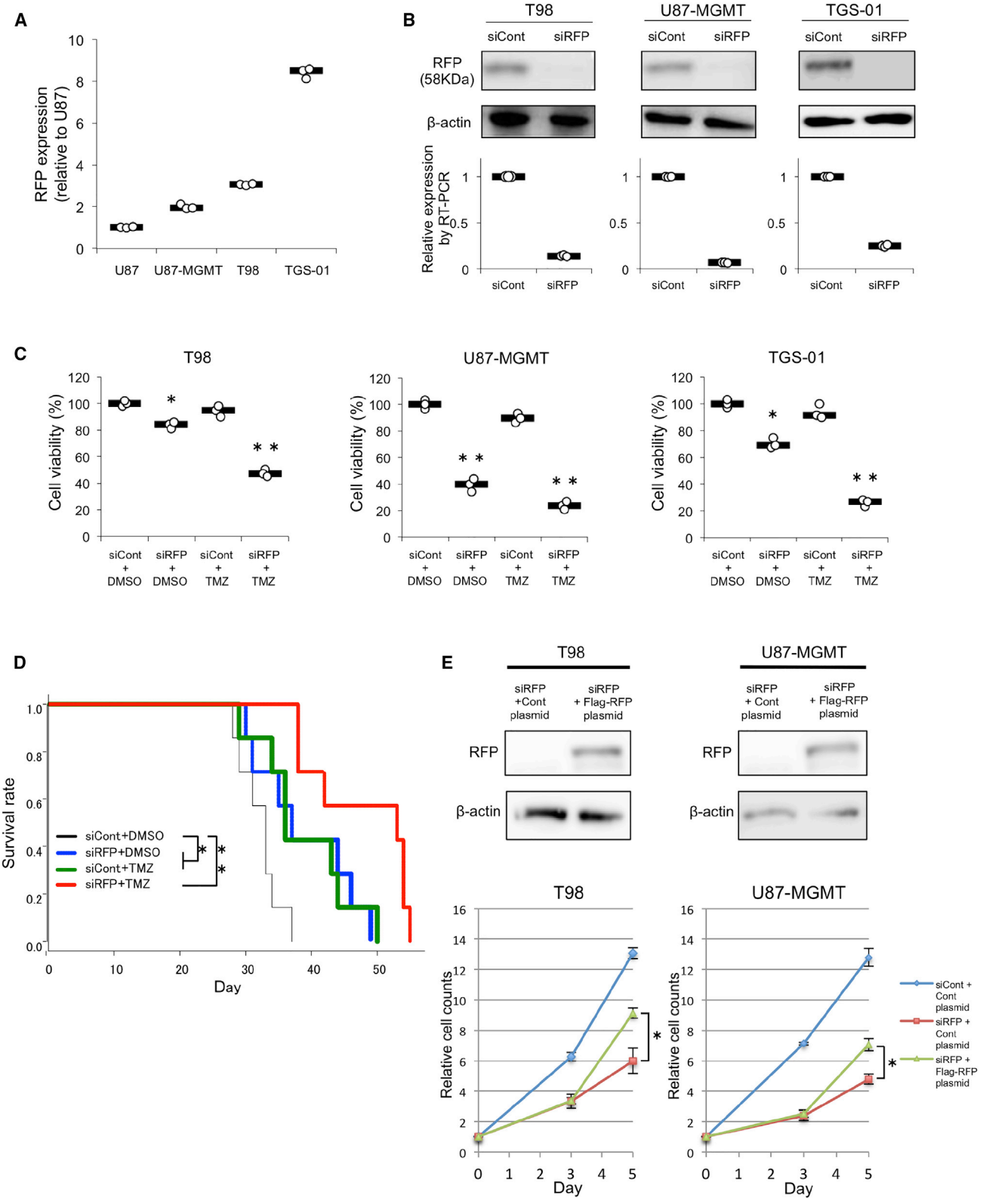

(legend on next page)

RESULTS

RFP siRNA Increases the Efficacy of TMZ against RFP-Expressing Glioma Cells

U87 cells transduced with the *MGMT* gene (U87-MGMT), T98 cells, and a patient-derived GBM cell line (TGS-01) are all TMZ-resistant cell lines that express MGMT. We observed that the expression of RFP was higher in these cell lines than in the U87 cell line, which does not express MGMT (Figure 1A). Western blotting and real-time PCR after transfection with RFP siRNA (siRFP) indicated that the expression of RFP in the transfected cells was suppressed (Figures 1B and S1A). Cell viability was evaluated after treatment with siRFP, TMZ, or both. The combination of siRFP with TMZ treatment increased the toxicity of TMZ toward all three cell lines. The highest cytotoxicity was observed with siRFP plus TMZ, compared to control siRNA (siCont) plus DMSO, siRFP plus DMSO, and siCont plus TMZ (Figure 1C). In the mouse model of a U87-MGMT orthotropic xenograft, the effect of siRFP combined with TMZ on mouse survival was consistent with the effect observed in the tumor cell viability assay *in vitro* (Figure 1D). Contrary to our expectations (Kato et al., 2009; Horio et al., 2012), siRFP alone significantly suppressed cell growth and survival. The RFP expression plasmid rescued the cell growth suppressed by siRFP (Figure 1E). These findings suggested that RFP-KD overcomes chemoresistance to TMZ and modifies a cellular process related to cell death mediated by certain machineries.

RFP-KD Impairs *cis*-Regulatory Elements That Control the Genes Regulating Cell Division, DNA Replication, the Cell Cycle, and Apoptosis

RFP formed a complex with HDAC1 in GBM cells (Figure 2A) just as in HeLa cells (Kato et al., 2009). Next, we focused on the aberrant H3K27ac-controlled active *cis*-regulatory elements as a consequence of RFP-HDAC1 disruption by RFP-KD. H3K27ac distinguishes active from poised and inactive regulatory elements (Creyghton et al., 2010). We performed H3K27ac chromatin immunoprecipitation with high-throughput sequencing (ChIP-seq) to identify RFP-HDAC1-controlled active and inactive elements regulating gene expression. RFP-KD resulted in changes in H3K27ac enrichment, which correlated with changes in RNA expression levels of the adjacent genes, as quantified by high-throughput sequencing of RNA (RNA-seq) (Figure 2B). The number of genes that gained H3K27ac (>1.5-fold) and manifested significantly increased fragments per kilobase of transcript per million mapped reads (FPKM) in both cell lines was 62, whereas that of genes with H3K27ac loss (<2/3-fold) and significantly diminished FPKM was 293. Gene Ontology (GO) analysis suggested that genes responsible for apoptosis were upregulated, and genes controlling mitotic cell activity, the cell cycle, and DNA replication were downregulated in RFP-depleted glioma cells (Figure 2C). Of note, among the genes that were designated as "H3K27ac gain" under the influence of siRFP, RNA levels of TBP-2 (TXNIP) and FOXO1 underwent a significant increase as compared to group siControl (3.7-fold and 3.9-fold in U87-MGMT cells, and 2.1-fold and 1.2-fold in T98 cells, respectively) (Figure 2D; Table S1). On the other hand, among the genes designated as "H3K27ac loss," RNA levels of PARPBP were significantly decreased by siRFP (0.2-fold in U87-MGMT cells and 0.76-fold in T98 cells) (Figure 2E; Table S2). After an experiment designed to show that HDAC1-RFP cooperated with the *cis*-regulatory elements, HDAC1- and RFP-ChIP with qPCR, respectively, showed significant coenrichment of HDAC1 and RFP in the "H3K27ac gain" regions adjacent to the corresponding upregulated genes (*TGM2*, *TXNIP*, *TNFRSF21*, and *FOXO1*) (Figure 2F). Nonetheless, significant enrichment of RFP was not detected in the "H3K27ac loss" region adjacent to downregulated genes (*NDRG1*, *KPNA2*, *TOP2A*, and *PARPBP*) (Figure 2G).

RFP and PARPBP Expression Correlates with Poor Prognosis in Patients with Glioma

We supposed that RFP-KD removed the H3K27ac mark in the region around *PARPBP*, thus resulting in a decrease in its expression (Figure 2E). PARP-1 is known to be a key BER protein in one of the repair mechanisms involving TMZ resistance (Curtin et al., 2004). In addition, large amounts of PARPBP have been detected in other cancers (Piao et al., 2011). It has been reported previously that PARP inhibition increases the efficacy of TMZ (Piao et al., 2011). Next, we investigated the possible clinical impact of PARPBP on the survival of patients with glioma. Upon analysis of a TCGA (The Cancer Genome Atlas) glioma dataset (Ceccarelli et al., 2016), we observed that the expression level of RFP significantly correlated with the overall survival of patients with glioma (Figure 3A). Similarly, the expression level of PARPBP also significantly correlated with the overall survival of patients with glioma (Figure 3B). Therefore, we inferred that RFP-KD may increase TMZ efficacy at least in part by inhibiting the activity of the PARPBP-PARP1 complex (Figure S2A).

RFP-KD Induces Oxidative Stress Leading to Apoptosis and Inhibiting Cell Division

ChIP-seq and RNA-seq after RFP-KD and GO analysis revealed that disruption of the RFP-HDAC1 complex dramatically

Figure 1. siRFP Increases the Efficacy of TMZ in RFP-Expressing Glioma Cells

(A) RFP expression was high in MGMT-expressing and TMZ-resistant glioma cell lines T98, U87-MGMT, and TGS-01, compared to the MGMT null U87 cell line.

(B) Liposome-mediated transfection of siRFP into glioma cell lines T98, U87-MGMT, and TGS-01. The RFP knockdown (KD) was confirmed by western blotting and qPCR (see also Figure S1A).

(C) The viability of glioma cell lines T98, U87-MGMT, and TGS-01 transfected with siRFP was assessed after treatment with TMZ. The combination of siRFP and TMZ treatment yielded the lowest cell viability. *$p < 0.05$, **$p < 0.01$, compared to siCont plus DMSO.

(D) The combined treatment with siRFP and TMZ had a consistent effect on the survival of mice with the U87-MGMT orthotropic xenograft. *$p < 0.05$, **$p < 0.01$, compared to siCont plus DMSO.

(E) A rescue assay. Addition of a plasmid (pFlag-RFP) on day 3 recovered cell proliferation in glioma cells treated with siRFP on day 1. Error bars represent ± SD. *$p < 0.05$.

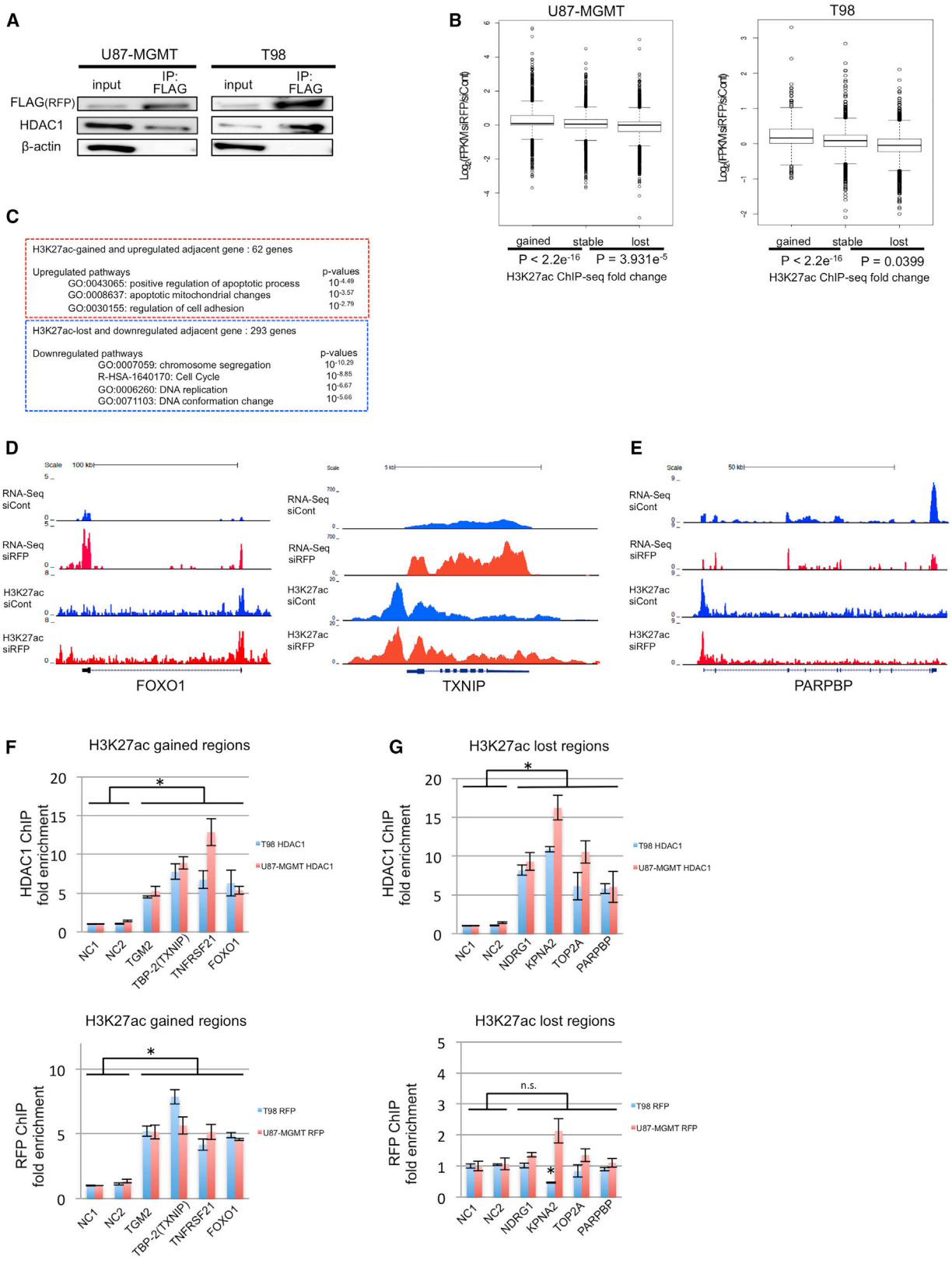

(legend on next page)

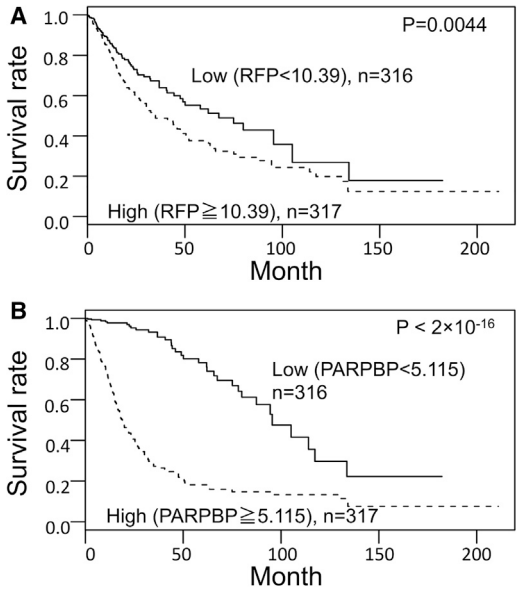

Figure 3. RFP and PARPBP Expression Correlates with Poor Prognosis in Patients with Glioma

(A) RFP expression correlates with poor prognosis in patients with glioma. Overall survival of 633 patients with glioma was stratified by expression of RFP: $\log_2$(RPKM + 0.001), cutoff = 10.39 (median), and analyzed by means of a Kaplan-Meier plot.

(B) PARPBP expression correlates with poor prognosis in patients with glioma: $\log_2$(RPKM + 0.001), cutoff = 5.115 (median), and analysis via a Kaplan-Meier plot.

changed H3K27ac status and expression of genes related to cell death and DNA replication (Figures 2B and 2C). We tested whether siRFP and/or TMZ induced oxidative stress in U87-MGMT, T98, and TGS-01 cells. CellROX Orange staining and examination by fluorescence microscopy showed that oxidative stress significantly increased in cells treated with siRFP and/or TMZ (Figures 4A and S1B). The staining of cells with CellROX and MitoTracker implicated a site other than the mitochondria (most likely, the cell membrane) as the primary source of reactive oxygen species (ROS) (Figure 4B). RFP-KD alone decreased the percentage of cells in the S phase and at the G2-M transition and increased the percentage of cells at the G0-G1 transition. TMZ alone increased the percentage of cells at the G2-M transition (Figure 4C). RFP-KD alone inhibited cell cycle progression, independently of TMZ treatment. Analysis of apoptotic cell death by a terminal deoxynucleotidyl transferase dUTP nick end labeling (TUNEL) assay revealed that a combination of siRFP and TMZ induced apoptosis (Figure 4D).

DISCUSSION

We demonstrated that disruption of the RFP-HDAC1 complex disordered the functioning of H3K27ac-controlled active *cis*-regulatory elements. We also assessed chemoresistance in TMZ-resistant gliomas and found that RFP-KD increased the anticancer efficacy of TMZ.

At first, we expected that the depletion of RFP-HDAC1 would lead to upregulation of H3K27ac in most *cis*-regulatory-element regions. We did detect increases in H3K27ac amounts in some regions, but we also found decreases in H3K27ac amounts in other regions. The results of HDAC1- and RFP-ChIP-qPCR implied that the RFP-HDAC1 complex directly controls the "H3K27ac gain" and upregulated genes, but controls the "H3K27ac loss" and downregulated genes indirectly, and the precise mechanism remains to be explained. After analyzing the genes in the "H3K27ac loss" group, whose expression level significantly decreased, we found that they included genes with functions in the cell cycle, cell division, and DNA replication. We then performed additional experiments on the cell cycle to evaluate the pertinence of these genes to our study and found that RFP-KD decreased the percentages of cells in the S phase and at the G2-M transition.

We found higher expression of RFP in TMZ-resistant cell lines that express MGMT. Possibly, RFP-KD decreases TMZ resistance by decreasing MGMT expression or activity. RFP binds to PML (Cao et al., 1998), and PML interacts with the mSin3a-HDAC1 corepressor (Khan et al., 2001), which in turn is known to inhibit MGMT expression (Bobustuc et al., 2010). Furthermore, RFP is linked with p53 sumoylation (Matsuura et al., 2005; Blough et al., 2007), and p53 downregulates MGMT in astrocytes (Blough et al., 2007). Our findings of RFP's association with prognosis, overall survival, and chemoresistance in glioma suggest that RFP is a potential therapeutic target in higher-grade astrocytic glioma. Nevertheless, our results suggested that the effects of RFP-KD on TMZ sensitivity were synergistic in T98 and TGS-01 cells but additive in U87-MGMT cells. Thus, we assumed that this difference may not be due only to MGMT-mediated chemoresistance.

The PARPBP-PARP1 complex is a key BER agent causing TMZ resistance. We observed that RFP-KD led to a significant

Figure 2. RFP-KD Impairs *cis*-Regulatory Element-Mediated Regulation of Genes Related to Cell Division, the Cell Cycle, DNA Replication, and Apoptosis

(A) U87-MGMT and T98 cells were transfected with the pFlag-RFP expression plasmid. Immunoprecipitates made with the anti-FLAG antibody were analyzed by western blotting with the indicated antibodies, showing that RFP forms a complex with HDAC1 in both cell lines.

(B) Regions of enrichment (RoEs) with the marker H3K27ac of active *cis*-regulatory elements were located by means of ChIP in U87-MGMT and T98 cells with the RFP-KD. Corresponding gene expression levels were determined by RNA-seq.

(C) GO analysis suggests that RFP-KD upregulates apoptosis and downregulates the pathways for cell division, the cell cycle, and DNA replication in glioma cells.

(D) Gene expression levels and H3K27ac peaks of thioredoxin binding protein-2 (TBP-2, TXNIP) and FOXO1 in U87-MGMT cells. Both are activated after RFP-KD, with an increase of more than 1.5-fold; scale bars represent 100kb for FOXO and 5kb for TXNIP.

(E) The gene expression level and H3K27ac peaks of PARPBP in U87-MGMT cells; scale bars represent 50kb.

(F) ChIP-qPCR reveals significant coenrichment of HDAC1 and RFP in the "H3K27ac gain" regions adjacent to the indicated genes; scale bars represent ± SD.

(G) ChIP-qPCR indicates no significant enrichment of RFP but significant enrichment of HDAC1 in the "H3K27ac loss" regions adjacent to the indicated genes; scale bars represent ± SD. *$p < 0.05$; n.s., not significant.

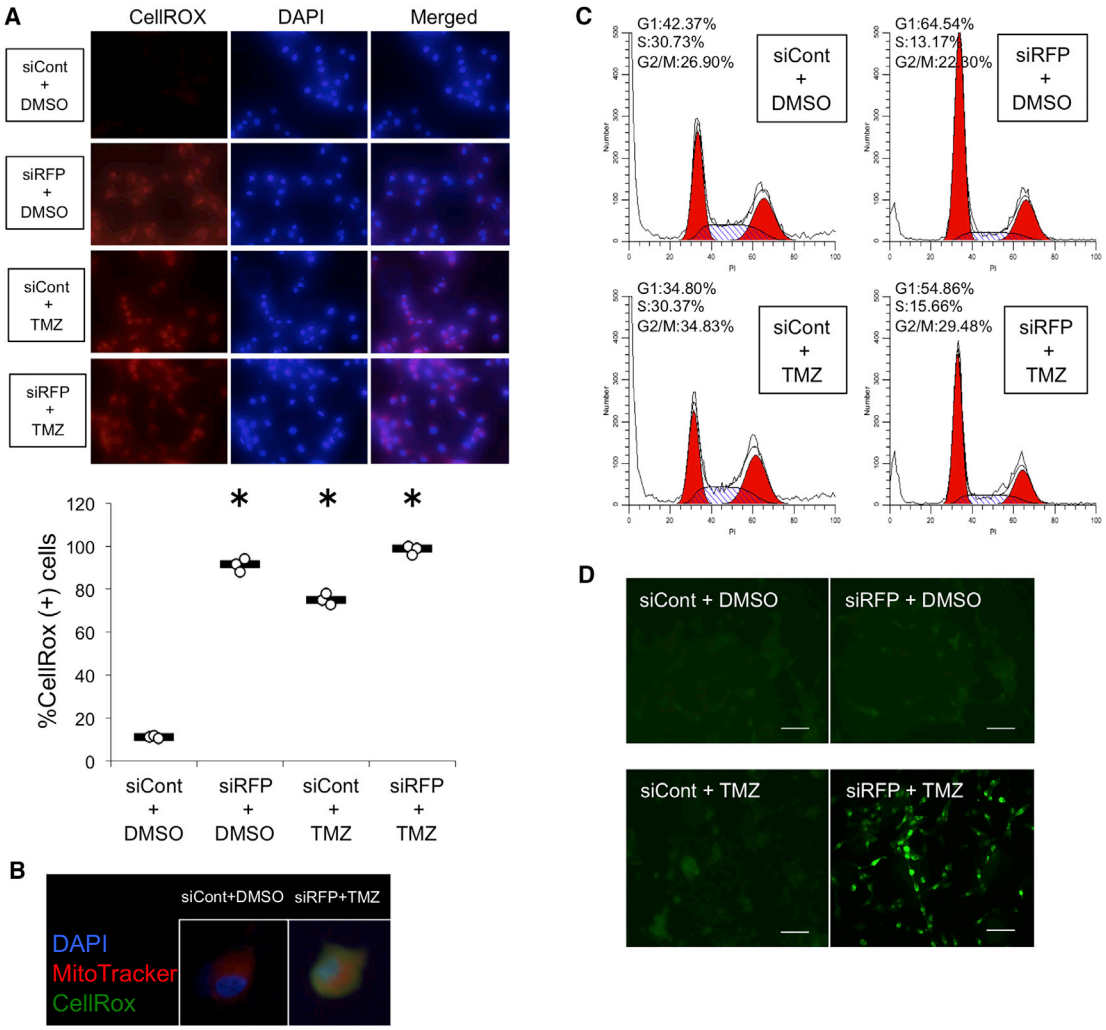

Figure 4. RFP-KD Induces Oxidative Stress Leading to Apoptosis and Inhibition of Cell Division

(A) siRFP+TMZ-treated cells manifest increased oxidative stress. More than 80% of U87-MGMT cells treated with siRFP and/or TMZ showed fluorescence in a CellROX Orange assay, indicating an increase in oxidative stress. *$p < 0.05$ compared to group "siCont plus DMSO" (see also Figure S1B).

(B) Confocal microscopy after CellROX Green and MitoTracker assays indicates that the source of ROS is primarily in the cell membrane.

(C) Cell-cycle analysis suggests that siRFP alone decreased the percentage of cells in the S and G2/M phase, and increased the percentage of cells in the G0/G1 phase in U87-MGMT cells. TMZ alone increased the percentage of cells in the G2/M phase.

(D) TUNEL assay showed that the combination of siRFP and TMZ induced apoptosis in U87-MGMT cells; scale bars represent 50 μm.

decrease in PARPBP expression. In addition, it has been observed that PARP1 inhibitors sensitize other cancers to anti-tumor agents via inhibition of thioredoxin (TRX) and ROS production (Yin et al., 2017).

RFP-KD disrupts the RFP-HDAC1 complex, resulting in an increase in FOXO1 and TBP-2 amounts, generating ROS and inducing apoptosis. HDAC1 inhibits FOXO1 (Yang et al., 2009), which induces the expression of TBP-2. Overexpression of TBP-2 therefore results in inactivation of *TRX* and an increase in oxidative stress (Kato et al., 2009). RFP-KD inhibited HDAC1. This action resulted in increased expression of FOXO1 and TBP-2 (TXNIP) (Figure S2B). TMZ treatment alone also increased oxidative stress in U87-MGMT and T98 cells, but our findings revealed that the combination of RFP-KD and TMZ treatment is more effective.

Therefore, we can conclude that RFP-KD or the disruption of the RFP-HDAC1 complex leads to increased chemosensitivity to TMZ in GBM by altering the pattern of histone modifications, thereby leading to changes in oxidative stress and cell division.

STAR★METHODS

Detailed methods are provided in the online version of this paper and include the following:

- KEY RESOURCES TABLE
- CONTACT FOR REAGENT AND RESOURCE SHARING

SUPPLEMENTAL INFORMATION

Supplemental Information can be found with this article online at https://doi.org/10.1016/j.celrep.2019.01.109.

ACKNOWLEDGMENTS

Computations were partially performed on the NIG supercomputer at ROIS National Institute of Genetics. This work was supported by a Grant-in-Aid for Scientific Research on Innovative Areas "Chemistry for Multimolecular Crowding Biosystems" (JSPS KAKENHI Grant 17928985).

AUTHOR CONTRIBUTIONS

Conceptualization, A.N.; Methodology, A.N. and F.O.; Investigation, M.R., M.H., A.K., S.M., T.K., F.O., and A.Y.; Validation, M.R. and M.H.; Data Curation, M.H. and Y.O.; Formal Analysis, M.R., M.H., Y.O., and K. Matsuo; Writing – Original Draft, M.R., A.N., and M.H.; Writing – Review & Editing, M.R., A.N., M.H., F.O., K.A., T.K., and A.E.; Visualization, M.H., M.R., and A.N.; Resources, T.K., M.T., Y.O., T.T., Y.I., and K. Matsuo; Funding Acquisition, A.N.; Supervision, A.N., K. Motomura, M.T., and T.W.

DECLARATION OF INTERESTS

The authors declare no competing interests.

Received: July 12, 2018
Revised: January 6, 2019
Accepted: January 29, 2019
Published: February 26, 2019

REFERENCES

Blough, M.D., Zlatescu, M.C., and Cairncross, J.G. (2007). O^6-methylguanine-DNA methyltransferase regulation by p53 in astrocytic cells. Cancer Res. *67*, 580–584.

Bobustuc, G.C., Baker, C.H., Limaye, A., Jenkins, W.D., Pearl, G., Avgeropoulos, N.G., and Konduri, S.D. (2010). Levetiracetam enhances p53-mediated MGMT inhibition and sensitizes glioblastoma cells to temozolomide. Neuro-oncol. *12*, 917–927.

Cao, T., Duprez, E., Borden, K.L., Freemont, P.S., and Etkin, L.D. (1998). Ret finger protein is a normal component of PML nuclear bodies and interacts directly with PML. J. Cell Sci. *111*, 1319–1329.

Ceccarelli, M., Barthel, F.P., Malta, T.M., Sabedot, T.S., Salama, S.R., Murray, B.A., Morozova, O., Newton, Y., Radenbaugh, A., Pagnotta, S.M., et al.; TCGA Research Network (2016). Molecular profiling reveals biologically discrete subsets and pathways of progression in diffuse glioma. Cell *164*, 550–563.

Creyghton, M.P., Cheng, A.W., Welstead, G.G., Kooistra, T., Carey, B.W., Steine, E.J., Hanna, J., Lodato, M.A., Frampton, G.M., Sharp, P.A., et al. (2010). Histone H3K27ac separates active from poised enhancers and predicts developmental state. Proc. Natl. Acad. Sci. USA *107*, 21931–21936.

Curtin, N.J., Wang, L.Z., Yiakouvaki, A., Kyle, S., Arris, C.A., Canan-Koch, S., Webber, S.E., Durkacz, B.W., Calvert, H.A., Hostomsky, Z., and Newell, D.R. (2004). Novel poly(ADP-ribose) polymerase-1 inhibitor, AG14361, restores sensitivity to temozolomide in mismatch repair-deficient cells. Clin. Cancer Res. *10*, 881–889.

Goldman, M., Craft, B., Swatloski, T., Ellrott, K., Cline, M., Diekhans, M., Ma, S., Wilks, C., Stuart, J., Haussler, D., and Zhu, J. (2013). The UCSC Cancer Genomics Browser: update 2013. Nucleic Acids Res. *41*, D949–D954.

Hasegawa, N., Iwashita, T., Asai, N., Murakami, H., Iwata, Y., Isomura, T., Goto, H., Hayakawa, T., and Takahashi, M. (1996). A RING finger motif regulates transforming activity of the rfp/ret fusion gene. Biochem. Biophys. Res. Commun. *225*, 627–631.

Heinz, S., Benner, C., Spann, N., Bertolino, E., Lin, Y.C., Laslo, P., Cheng, J.X., Murre, C., Singh, H., and Glass, C.K. (2010). Simple combinations of lineage-determining transcription factors prime *cis*-regulatory elements required for macrophage and B cell identities. Mol. Cell *38*, 576–589.

Heinz, S., Romanoski, C.E., Benner, C., and Glass, C.K. (2015). The selection and function of cell type-specific enhancers. Nat. Rev. Mol. Cell Biol. *16*, 144–154.

Hermisson, M., Klumpp, A., Wick, W., Wischhusen, J., Nagel, G., Roos, W., Kaina, B., and Weller, M. (2006). O^6-methylguanine DNA methyltransferase and p53 status predict temozolomide sensitivity in human malignant glioma cells. J. Neurochem. *96*, 766–776.

Horio, M., Kato, T., Mii, S., Enomoto, A., Asai, M., Asai, N., Murakumo, Y., Shibata, K., Kikkawa, F., and Takahashi, M. (2012). Expression of RET finger protein predicts chemoresistance in epithelial ovarian cancer. Cancer Med. *1*, 218–229.

Ikushima, H., Todo, T., Ino, Y., Takahashi, M., Miyazawa, K., and Miyazono, K. (2009). Autocrine TGF-beta signaling maintains tumorigenicity of glioma-initiating cells through Sry-related HMG-box factors. Cell Stem Cell *5*, 504–514.

Isomura, T., Tamiya-Koizumi, K., Suzuki, M., Yoshida, S., Taniguchi, M., Matsuyama, M., Ishigaki, T., Sakuma, S., and Takahashi, M. (1992). RFP is a DNA binding protein associated with the nuclear matrix. Nucleic Acids Res. *20*, 5305–5310.

Iwakoshi, A., Murakumo, Y., Kato, T., Kitamura, A., Mii, S., Saito, S., Yatabe, Y., and Takahashi, M. (2012). RET finger protein expression is associated with prognosis in lung cancer with epidermal growth factor receptor mutations. Pathol. Int. *62*, 324–330.

Kato, T., Shimono, Y., Hasegawa, M., Jijiwa, M., Enomoto, A., Asai, N., Murakumo, Y., and Takahashi, M. (2009). Characterization of the HDAC1 complex that regulates the sensitivity of cancer cells to oxidative stress. Cancer Res. *69*, 3597–3604.

Khan, M.M., Nomura, T., Kim, H., Kaul, S.C., Wadhwa, R., Shinagawa, T., Ichikawa-Iwata, E., Zhong, S., Pandolfi, P.P., and Ishii, S. (2001). Role of PML and PML-RARalpha in Mad-mediated transcriptional repression. Mol. Cell *7*, 1233–1243.

Kim, D., Pertea, G., Trapnell, C., Pimentel, H., Kelley, R., and Salzberg, S.L. (2013). TopHat2: accurate alignment of transcriptomes in the presence of insertions, deletions and gene fusions. Genome Biol. *14*, R36.

Langmead, B., and Salzberg, S.L. (2012). Fast gapped-read alignment with Bowtie 2. Nat. Methods *9*, 357–359.

Marks, P.A., Miller, T., and Richon, V.M. (2003). Histone deacetylases. Curr. Opin. Pharmacol. *3*, 344–351.

Matsuura, T., Shimono, Y., Kawai, K., Murakami, H., Urano, T., Niwa, Y., Goto, H., and Takahashi, M. (2005). PIAS proteins are involved in the SUMO-1 modification, intracellular translocation and transcriptional repressive activity of RET finger protein. Exp. Cell Res. *308*, 65–77.

McNab, F.W., Rajsbaum, R., Stoye, J.P., and O'Garra, A. (2011). Tripartite-motif proteins and innate immune regulation. Curr. Opin. Immunol. *23*, 46–56.

Mottet, D., and Castronovo, V. (2008). Histone deacetylases: target enzymes for cancer therapy. Clin. Exp. Metastasis *25*, 183–189.

Piao, L., Nakagawa, H., Ueda, K., Chung, S., Kashiwaya, K., Eguchi, H., Ohigashi, H., Ishikawa, O., Daigo, Y., Matsuda, K., and Nakamura, Y. (2011). C12orf48, termed PARP-1 binding protein, enhances poly(ADP-ribose) polymerase-1 (PARP-1) activity and protects pancreatic cancer cells from DNA damage. Genes Chromosomes Cancer *50*, 13–24.

Reymond, A., Meroni, G., Fantozzi, A., Merla, G., Cairo, S., Luzi, L., Riganelli, D., Zanaria, E., Messali, S., Cainarca, S., et al. (2001). The tripartite motif family identifies cell compartments. EMBO J. *20*, 2140–2151.

Shimono, Y., Murakami, H., Hasegawa, Y., and Takahashi, M. (2000). RET finger protein is a transcriptional repressor and interacts with enhancer of polycomb that has dual transcriptional functions. J. Biol. Chem. *275*, 39411–39419.

Stupp, R., Mason, W.P., van den Bent, M.J., Weller, M., Fisher, B., Taphoorn, M.J.B., Belanger, K., Brandes, A.A., Marosi, C., Bogdahn, U., et al.; European Organisation for Research and Treatment of Cancer Brain Tumor and Radiotherapy Groups; National Cancer Institute of Canada Clinical Trials Group (2005). Radiotherapy plus concomitant and adjuvant temozolomide for glioblastoma. N. Engl. J. Med. *352*, 987–996.

Stupp, R., Hegi, M.E., Mason, W.P., van den Bent, M.J., Taphoorn, M.J., Janzer, R.C., Ludwin, S.K., Allgeier, A., Fisher, B., Belanger, K., et al.; European Organisation for Research and Treatment of Cancer Brain Tumour and Radiation Oncology Groups; National Cancer Institute of Canada Clinical Trials Group (2009). Effects of radiotherapy with concomitant and adjuvant temozolomide versus radiotherapy alone on survival in glioblastoma in a randomised phase III study: 5-year analysis of the EORTC-NCIC trial. Lancet Oncol. *10*, 459–466.

Takahashi, M., Ritz, J., and Cooper, G.M. (1985). Activation of a novel human transforming gene, ret, by DNA rearrangement. Cell *42*, 581–588.

Takahashi, M., Inaguma, Y., Hiai, H., and Hirose, F. (1988). Developmentally regulated expression of a human "finger"-containing gene encoded by the 5′ half of the ret transforming gene. Mol. Cell. Biol. *8*, 1853–1856.

Tentori, L., Leonetti, C., Scarsella, M., D'Amati, G., Vergati, M., Portarena, I., Xu, W., Kalish, V., Zupi, G., Zhang, J., and Graziani, G. (2003). Systemic administration of GPI 15427, a novel poly(ADP-ribose) polymerase-1 inhibitor, increases the antitumor activity of temozolomide against intracranial melanoma, glioma, lymphoma. Clin. Cancer Res. *9*, 5370–5379.

Tezel, G., Nagasaka, T., Iwahashi, N., Asai, N., Iwashita, T., Sakata, K., and Takahashi, M. (1999). Different nuclear/cytoplasmic distributions of RET finger protein in different cell types. Pathol. Int. *49*, 881–886.

Trapnell, C., Hendrickson, D.G., Sauvageau, M., Goff, L., Rinn, J.L., and Pachter, L. (2013). Differential analysis of gene regulation at transcript resolution with RNA-seq. Nat. Biotechnol. *31*, 46–53.

Tsukamoto, H., Kato, T., Enomoto, A., Nakamura, N., Shimono, Y., Jijiwa, M., Asai, N., Murakumo, Y., Shibata, K., Kikkawa, F., and Takahashi, M. (2009). Expression of Ret finger protein correlates with outcomes in endometrial cancer. Cancer Sci. *100*, 1895–1901.

Yang, Y., Zhao, Y., Liao, W., Yang, J., Wu, L., Zheng, Z., Yu, Y., Zhou, W., Li, L., Feng, J., et al. (2009). Acetylation of FoxO1 activates Bim expression to induce apoptosis in response to histone deacetylase inhibitor depsipeptide treatment. Neoplasia *11*, 313–324.

Yin, Z.X., Hang, W., Liu, G., Wang, Y.S., Shen, X.F., Sun, Q.H., Li, D.D., Jian, Y.P., Zhang, Y.H., Quan, C.S., et al. (2017). PARP-1 inhibitors sensitize HNSCC cells to APR-246 by inactivation of thioredoxin reductase 1 (TrxR1) and promotion of ROS accumulation. Oncotarget *9*, 1885–1897.

Zhu, J., Sanborn, J.Z., Benz, S., Szeto, C., Hsu, F., Kuhn, R.M., Karolchik, D., Archie, J., Lenburg, M.E., Esserman, L.J., et al. (2009). The UCSC Cancer Genomics Browser. Nat. Methods *6*, 239–240.

STAR★METHODS

KEY RESOURCES TABLE

REAGENT or RESOURCE	SOURCE	IDENTIFIER
Antibodies		
Histone H3K27ac antibody	Active Motif	Cat# 39134; RRID:AB_2722569
Rabbit polyclonal anti-RFP antibody	Tezel et al., 1999; Immuno-Biological Laboratories	Cat# 18791
Anti-HDAC antibody	Cell signaling technology	Cat# 34589
Anti-HDAC antibody	Merck KGaA	Cat# 06-720
Anti-FLAG M2 antibody	Merck KGaA	Product# F-1804
Chemicals, Peptides, and Recombinant Proteins		
Temozolomide	Tokyo Chemical Industry Japan	Product no. T2744
Critical Commercial Assays		
Lipofectamine 3000	Invitrogen	Cat. No. L3000008
Lipofectamine RNAiMAX Transfection Reagent	Invitrogen	Cat. No. 13778150
ReverTrAce qPCR RT kit	Toyobo	Cat. No. FSQ-101
THUNDERBIRD SYBR qPCR Mix	Toyobo	Cat. No. QPS-201
GeneArt Site-Directed Mutagenesis PLUS System	Invitrogen	Cat. No. A14604
NEBNext Ultra II DNA library Prep kit for Illumina	New England Biolabs	Cat. No. E7645S
NEBNext Ultra RNA library Prep Kit for Illumina	New England Biolabs	Cat. No. E7530
NEBNext Poly(A) mRNA Magnetic Isolation Module	New England Biolabs	Cat. No. E7490
CellROX® Orange Reagent	Thermo Fisher Scientific	Cat. No. C10443
CellROX® Green Reagent	Thermo Fisher Scientific	Cat. No. C10444
MitoTracker® Red FM Reagent	Thermo Fisher Scientific	Cat. No.M22425
In situ apoptosis detection kit	TaKaRa	Cat. No. MK500
Deposited Data		
ChIP-seq data (Illumina HiSeq 2000 or MiSeq paired end sequencing)	This paper	DDBJ: DRA007944
RNA-seq data (Illumina HiSeq 2000 or MiSeq paired end sequencing)	This paper	DDBJ: DRA007944
Other raw data used for figures	This paper	https://data.mendeley.com/datasets/4pr6pd3g8k/draft?a=3af7451e-1f68-4776-a963-bf36c2a4d49a
Experimental Models: Cell Lines		
Human: T98	RIKEN Bioresource Research Center, Japan	RRID:CVCL_B368
Human: U87	Brain Tumor Research Center, UCSF	U-87MG ATCC (RRID:CVCL_0022)
Human: TGS-01	Todo Laboratory, the University of Tokyo; Ikushima et al., 2009	N/A
Experimental Models: Organisms/Strains		
Mouse: BALB/c nu/nu	Japan SLC	http://www.jslc.co.jp/pdf/mouse/014_balbnu2007.pdf
Oligonucleotides		
5′-GAGUUACUCGGGAGGGAAA-3′ (siRFP1)	Shimono et al., 2000	N/A
5′- GAGAGGCUCAGUUAUACU-3′ (siRFP2)	Shimono et al., 2000	N/A
5′- GACUCAGUGUGCAGAAAAG-3′ (siRFP3)	Shimono et al., 2000	N/A
5′-TGCTCGACTGCGGCCATAAC-3′ (RFP forward primer)	Shimono et al., 2000	N/A
5′-TCGGTGCGCAGCTGCTTTAC-3′ (RFP reverse primer)	Shimono et al., 2000	N/A

(*Continued on next page*)

Continued

REAGENT or RESOURCE	SOURCE	IDENTIFIER
Recombinant DNA		
wild-type pFlag-RFP plasmid	Shimono et al., 2000	N/A
pFlag-RFP plasmid with silent mutations	This paper	N/A
Software and Algorithms		
Trim Galore! v0.4.4	Babraham Bioinformatics	http://www.bioinformatics.babraham.ac.uk/projects/trim_galore/
FastQC	Babraham Bioinformatics	http://www.bioinformatics.babraham.ac.uk/projects/fastqc/
Bowtie2 v2.2.9	Langmead and Salzberg, 2012	RRID:SCR_016368
FindPeaks program, HOMER software package	University of California, San Diego	http://homer.ucsd.edu/homer/
makeUCSCfile program, HOMER software package.	University of California, San Diego	http://homer.ucsd.edu/homer/
TopHat v2.1.1	Kim et al., 2013	RRID:SCR_013035
Cufflinks v2.1.1	Trapnell et al., 2013	RRID:SCR_014597
EZ-R	Jichi Medical University Saitama Medical Center	http://www.jichi.ac.jp/saitama-sct/SaitamaHP.files/statmedEN.html
ModFit LT v3.3	BD Biosciences	Cat No.346033
Other		
ChIP-Atlas	National Bioscience Database Center, Kyushu University	RRID:SCR_015511
UCSC Cancer Genomics Browser	Goldman et al., 2013	http://xena.ucsc.edu/welcome-to-ucsc-xena/
The Cancer Genome Atlas (TCGA)	Ceccarelli et al., 2016	RRID:SCR_003193

CONTACT FOR REAGENT AND RESOURCE SHARING

Further information and requests for reagents may be directed to and will be fulfilled by the Lead Contact, Atsushi Natsume (anatsume@med.nagoya-u.ac.jp).

EXPERIMENTAL MODEL AND SUBJECT DETAILS

Mice

5-week-old female BALB/c nu/nu mice weighing 15-20 g were purchased from Japan SLC and subsequently housed under a strict 12-hour light/dark cycle in a specific pathogen free animal facility. Up to 4 mice were housed together in polypropylene cages with wire covers. Wood shavings were used as bedding and standard mouse food and sterile filtered water were provided *ad libitum*. Cages were changed every 3 days.

All animal procedures were in accordance to the guidelines of the Institutional Animal Care and Usage Committee of Nagoya University. The mice were anaesthetized with sodium pentobarbital (50mg/kg). U87-MGMT cells treated with siRNA for RFP (and siControl) were injected stereotactically, 3 mm right of the midline, 2 mm anterior to the coronal suture, and 3 mm deep into the right frontal lobes of mice, thus constructing orthotropic xenograft mouse models. DMSO or TMZ (50 mg/kg) dissolved in DMSO was injected intraperitoneally from day 2 to day 7. Specimens were evaluated by Kaplan Meier survival analysis.

Cell lines

Human glioma cell lines T98 (male), U87 (male) expressing MGMT (U87-MGMT, kindly provided by Prof. Russell Pieper of the University of California, San Francisco) were maintained in Dulbecco's modified Eagle's medium (DMEM) supplemented with 10% fetal bovine serum (FBS) and 1% penicillin-streptomycin (PS). TGS-01(male) cells (Ikushima et al., 2009) were maintained in DMEM/F12 supplemented with 2% B-27, 0.15% insulin. These cells were incubated at 37°C in a humidified atmosphere of 5% CO_2.

METHOD DETAILS

RNA interference and quantitative RT-PCR

RFP and control siRNAs were purchased from QIAGEN (QIAGEN, Hilden, Germany). The targeted sequences are as follows: 5′-GAG UUACUCGGGAGGGAAA-3′ (siRFP1), 5′- GAGAGGCUCAGUUAUACU-3′ (siRFP2), and 5′- GACUCAGUGUGCAGAAAAG-3′ (siRFP3).

T98 and U87-MGMT glioma cells were plated in 500 μL of DMEM with 10% FBS and 1% PS, at a density of 5×10^3 cells per well in a 24-well plate. TGS-01 cells were plated in 2mL of DMEM/F12 with 2% B-27, 0.15% insulin, at a density of 10^5 cells in a ultra-low attachment 60mm-dish. On day 1, siRNAs were transfected with Lipofectamine 3000 or Lipofectamine RNAiMAX (Invitrogen, Carlsbad, CA, USA) according to the manufacturer's instructions. Total RNA was extracted from cells with TRIzol reagent (Invitrogen) on day 4, and 500 ng of total RNA was reverse-transcribed using the ReverTra Ace qPCR RT kit (Toyobo, Osaka, Japan). The RFP forward and reverse primer sequences were 5′-TGCTCGACTGCGGCCATAAC-3′ and 5′-TCGGTGCGCAGCTGCTTTAC-3′, respectively. Lamin A/C PCR products from the same RNA samples were amplified and used for an internal control. cDNA was quantified with a spectrophotometer, diluted to 500 ng/μL, and used in real-time PCR. Real-time PCR was carried out using a THUNDERBIRD SYBR qPCR Mix (Toyobo). The PCR reaction was analyzed with a Roche LightCycler (Roche, Basel, Switzerland). The effectiveness of RFP knockdown was highest with siRFP1 in all cell lines (Figure S1A). Therefore, siRFP1 was used for all other experiments in this study.

Cell viability count

Glioma cell lines T98, U87-MGMT and TGS-01 were plated in triplicate as described above. On day 1, siRNA for RFP (siRFP) or control siRNA (siCont) was transfected. Temozolomide (TMZ) (200 μM) or dimethyl sulfoxide (DMSO) was added to the culture medium on day 3. On day 5, the number of cells in each well was counted using a Countess™ automated cell counter (Invitrogen, Thermo Fisher Scientific, Waltham, MA, USA).

siRNA rescue assay

The wild-type pFlag-RFP plasmid was constructed by cloning 3 fragments of RFP gene into the pGEM-T vector (Promega). The resulting full-length RFP gene was subcloned into the EcoRI/BamHI sites of the pFLAG-CMV2 vector (Shimono et al., 2000). It was mutagenized by PCR using GeneArt Site-Directed Mutagenesis PLUS System (Invitrogen) to generate pFlag-RFP plasmid that contains three silent mutations in the siRFP1 targeting sequence, CAGTTACTCCGGAGGC. The mutations were confirmed by sequence analysis.

T98 and U87-MGMT cells were plated in 2mL of DMEM with 10% FBS and 1% PS, at a density of 10^5 cells per well in a 6-well plate. On day 1, siRFP or siCont was transfected. On day 3, pFlag-RFP plasmid with silent mutations or control plasmid with siRNA was transfected with Lipofectamine 3000. On day 3 and day 5, the number of cells was counted as described above.

Sample preparation for ChIP-seq and ChIP-qPCR

U87-MGMT and T98 cells plated in a 100mm-dish and transfected with siRFP or siCont in duplicate, were cross-linked in 1% paraformaldehyde for 8 min, collected with a cell scraper, and washed three times with PBS. Chromatin was sheared with a Covaris sonicator (adaptive focused acoustics; AFA technology, Melaka, Malaysia). H3K27ac antibody (Active Motif, Tokyo, Japan), rabbit polyclonal anti-RFP antibody (Tezel et al., 1999) and anti-HDAC1 antibody (Cell Signaling TECHNOLOGY, MA, USA) were used for immunoprecipitation of sheared chromatin. Protein G dynabeads (Life Technologies, Carlsbad, CA, USA) were used to pull down the chromatin complexes. Complexes were digested with proteinase K, reverse cross-linked, and purified using Agencourt AMPure XP beads (BECKMAN COULTER, Brea, CA, USA).

Quantitative PCR (qPCR) was performed using SYBR qPCR Master mix (Toyobo, Japan) using 1% of purified ChIP DNA in triplicate. Primer design for ChIP-qPCR was based on ChIP-seq data of ChIP-Atlas (ChIP-Atlas, https://chip-atlas.org). Negative control primers used in this study were described previously (Kato et al., 2009) and are also summarized in Table S4. ChIP-qPCR signals were normalized using the percent input method (100 × 2^(adjusted input – Ct(IP))), and the values of fold enrichment were calculated using the ratio of the percent input for each primer set over negative control (NC) primer.

Fragmented ChIP DNA (1ng to 5 ng) was used to prepare DNA libraries for paired-end sequencing on the Miseq or Hiseq2000 (Illumina, San Diego, CA, USA) system, using the NEBNext Ultra II DNA library Prep kit for Illumina (New England Biolabs, Ipswich, MA, USA).

Sample preparation for RNA-seq

TRIzol Reagent (Life Technologies) was used to extract RNA from U87-MGMT and T98 cells transfected with siRFP or siCont from a 24-well plate, in triplicate. The quality and quantity of RNA were evaluated using NanoDrop 1000 spectrophotometer and Bioanalyzer 2100 (Agilent Technologies, CA, USA). In this study, all the RNA quality (RIN) scores were higher than 9.7. cDNA libraries for paired-end sequencing on the Miseq or Hiseq 2000 (Illumina) system were prepared using the NEBNext Ultra RNA library Prep Kit for Illumina (New England Biolabs), with the NEBNext Poly(A) mRNA Magnetic Isolation Module.

ChIP-seq processing

NGS reads sequenced with the Illumina MiSeq or HiSeq 2000 were trimmed to remove adapters and low-quality fragments by Trim Galore! v0.4.4 (http://www.bioinformatics.babraham.ac.uk/projects/trim_galore/) and evaluated by FastQC (http://www.bioinformatics.babraham.ac.uk/projects/fastqc/). Next, they were aligned to the hg19 genome assembly using Bowtie2 v2.2.9 (Langmead and Salzberg, 2012).

Different ChIP-seq regions of enrichment (RoEs) were identified using the FindPeaks program on the HOMER software package ('-style histone -size 1000 -minDist 2500' options), with matching input samples for each immunoprecipitation experiment (Heinz et al., 2010). As for the H3K27ac RoEs, the mean peak scores of each RoE in the siRFP group and siControl group (n = 2, respectively) were used for subsequent analyses. RoEs whose H3K27ac ChIP score increased by more than 1.5 fold were designated as 'gained', whereas the ones whose H3K27ac ChIP score decreased to less than 2/3 fold were designated as 'lost'. Furthermore, H3K27ac RoEs that were over 2 kb distal to TSS were defined as enhancers, whereas the ones proximal to TSS within 2 kb were defined as promoters in this study. The aligned ChIP-seq data were visualized using the makeUCSCfile program on the HOMER software package.

RNA-seq processing

NGS reads sequenced with the Illumina MiSeq or HiSeq 2000 were trimmed to remove adapters and low-quality fragments by Trim Galore! v0.4.4 (http://www.bioinformatics.babraham.ac.uk/projects/trim_galore/) and evaluated by FastQC (http://www.bioinformatics.babraham.ac.uk/projects/fastqc/). The sequenced reads were aligned to the hg19 genome + transcriptome assembly (UCSC hg19) using TopHat v2.1.1 (Kim et al., 2013) with default parameters. Expression values were calculated using Cufflinks v2.1.1 (Trapnell et al., 2013), and the values from siRFP group or siControl group were compared using Cuffdiff, ('–upper-quartile-norm' option). In this study, genes with FPKM < 1 in both siRFP group and siControl group were excluded, and only the genes corresponding to the H3K27ac peaks in which FPKM was significantly altered ($q < 0.05$) by RFP knockdown were used for subsequent analyses. The aligned RNA-seq data were visualized using the makeUCSCfile program on the HOMER software package.

Gene ontology analysis

Gene ontology (GO) analysis of 'gained' and 'lost' genes whose expression levels were significantly altered by RFP knockdown was performed using Metascape (http://metascape.org/).

Quality control of RNA-seq and ChIP-seq data

The total number of input reads was from 15.0 million to 67.2 million (RNA-seq) and 10.4 million to 31.4 million (ChIP-seq) (Table S3). All the mean Phred scores of the quality-filtered sequenced reads were more than 33. There were no overrepresented sequences, significant duplicated sequences and adaptor contents. The concordant pair alignment rate was from 70.6% to 87.1% (RNA-seq) and 90.5% to 96.9% (ChIP-seq) (Table S3).

Overall survival analysis of patients with glioma

Gene expression data was obtained from UCSC Cancer Genomics Browser (http://xena.ucsc.edu/welcome-to-ucsc-xena/) (Goldman et al., 2013; Zhu et al., 2009). In this data, expression level of each gene is represented as $\log_2$(RPKM+0.001). We used the latest clinical data from The Cancer Genome Atlas (TCGA) (Ceccarelli et al., 2016) for the analysis of overall survival of patients with glioma. Kaplan-Meier curves for two distinct groups of patients were plotted using survfit function in survival package of R v3.3.3. P value from log rank test was computed using survdiff function.

Immunoprecipitation

T98 and U87-MGMT cells plated in 100 mm dishes were transfected with 12.5 μg of pFLAG-RFP expression plasmid using Lipofectamine 3000 (Invitrogen) according to the manufacturer's instructions. After 48 h of incubation, cells were washed twice with ice-cold PBS and resuspended in 1 mL of RIPA buffer (50 mM Tris-HCl pH 7.4, 150 mM NaCl, 1 mM ZnCl2, 1% NP-40, 0.1% SDS, 1 mM DTT), containing EDTA-free complete protease inhibitor mixture (Roche Diagnostics, IN, USA) for 30 min. After brief sonication and centrifugation at 14,000 rpm for 10 min at 4°C, the supernatant was incubated with mouse anti-FLAG M2 antibody (Merck KGaA, Darmstadt, Germany) overnight. Protein G dynabeads were added for 2 h at 4°C and then 200 μL of 2 × SDS sample buffer with 10% of mercaptoethanol was added for 5 min at 100°C.

Western blot analysis

Total cell lysates (20 μg) were separated using a 10% SDS-polyacrylamide gel and transferred to an Amersham Hybond-P PVDF membrane (GE Healthcare Life Sciences, Uppsala, Sweden). After treatment with blocking solution [5% skimmed milk/0.1% Tween-20/phosphate-buffered saline (T-PBS)], the membranes were incubated overnight with manufacturer recommended dilution of the following primary antibodies: rabbit polyclonal anti-RFP antibody (Tezel et al., 1999), anti-HDAC1 antibody (Merck KGaA, Darmstadt, Germany), anti-FLAG antibody (Merck), and anti-beta actin antibody (Sigma-Aldrich). The membranes were washed three times for 15 min each with 0.1% T-PBS and then incubated with appropriate secondary antibody for 1 h. After washing with T-PBS, proteins were visualized using Amersham enhanced chemiluminescence prime western blotting detection reagent (GE Healthcare Life Sciences, Uppsala, Sweden) and detected with LAS 4000 mini Luminescent Image Analyzer (Fujifilm, Tokyo, Japan).

Oxidative stress levels and localization of ROS

CellROX® Orange and CellROX® Green Reagents (Thermo Fisher Scientific, Waltham, MA, USA) were added to T98, U87-MGMT and TGS-01 cells, and treated as described above, along with siRNA for RFP and TMZ in triplicate. The cells were incubated at 37°C for 30 min. After washing three times in PBS, MitoTracker® Red FM reagent (Thermo Fisher Scientific, Waltham, MA, USA)

was added to the cells according to the manufacturer's instruction, along with nuclear stain reagent DAPI (4′,6-diamidino-2-phenylindole). The cells were counted under fluorescence microscopes (Olympus, Tokyo, Japan and BZ-X700, KEYENCE, Osaka, Japan).

Cell cycle analysis

T98 and U87-MGMT cells treated as described above were fixed in 70% ethanol (−20°C) and resuspended in propidium iodide staining solution (5 μg/mL propidium iodide, 250 μg/mL RNase). Cytofluorimetric acquisitions were performed by BD FACS Canto™ II flow cytometer (BD, Franklin Lakes, NJ, USA), and data analysis was performed using ModFit LT v3.3 (BD).

Apoptosis analysis

Terminal deoxynucleotidyl transferase mediated dUTP-digoxigenin nick-end labeling (TUNEL) assays were performed on U87-MGMT cells and treated as described above to evaluate treatment-mediated apoptosis. The TUNEL assay was performed using an *in situ* apoptosis detection kit (TaKaRa, Shiga, Japan) according to the manufacturer's instruction.

QUANTIFICATION AND STATISTICAL ANALYSIS

For the data reported in Figure 1C, cell lines were plated in triplicate and analyzed by the t test. * $p < 0.05$, ** $p < 0.01$, compared to siCont + DMSO.

n = 7 in the data reported in Figure 1D. Mouse survival was evaluated by Kaplan Meier survival analysis and the Chi-square test using the software EZ-R. * $p < 0.05$, ** $p < 0.01$, compared to siCont + DMSO.

For the data in Figure 1E, cells transfected with siRNA plasmid, in triplicate, were counted and analyzed by the t test. * $p < 0.05$

For the data in Figure 2B, expression values of genes were calculated using Cufflinks, and the values from siRFP group or siControl group were compared using Cuffdiff (n = 3, biological replicates). $q < 0.05$ was defined as statistically significant. The Wilcoxon rank-sum test was used to test the significance of differences among H3K27ac 'gained', 'stable' and 'lost' groups.

For the ChIP-qPCR data shown in Figures 2F and 2G, the t test was used (n = 3, biological replicates). * $p < 0.05$

n = 633 for the data reported in Figure 3A. OS stratification of glioma patients was shown by expression of RFP [$\log_2$(RPKM + 0.001), cutoff = 10.39 (median)] and Kaplan-Meier analysis was done using survfit function in survival package of R v3.3.3. In Figure 3B, OS of glioma patients (n = 633) was stratified by the expression of PARPBP [$\log_2$(RPKM + 0.001), cutoff = 5.115 (median)]. Kaplan-Meier survival analysis was done using survfit function in survival package of R v3.3.3. P value from log rank test was computed using survdiff function.

For the data regarding oxidative stress reported in Figure 4A, the t test was used for statistical analysis (n = 3, biological replicates). * $p < 0.05$ as compared to group "siCont + DMSO."

DATA AND SOFTWARE AVAILABILITY

The accession number for the ChIP-seq and RNA-seq data reported in this study is DDBJ: DRA007944. Parent directory includes datasets for ChIP-seq (n = 12) and RNA-seq (n = 12). Other raw data used in this study are available at https://data.mendeley.com/datasets/4pr6pd3g8k/draft?a=3af7451e-1f68-4776-a963-bf36c2a4d49a.

Trim Galore! v0.4.4 (http://www.bioinformatics.babraham.ac.uk/projects/trim_galore/), FastQC (http://www.bioinformatics.babraham.ac.uk/projects/fastqc/), Bowtie2 v2.2.9 (Langmead and Salzberg, 2012) the FindPeaks program and the makeUCSCfile program on the HOMER software package (http://homer.ucsd.edu/homer/) were used for ChIP-seq analysis.

Trim Galore! v0.4.4 (http://www.bioinformatics.babraham.ac.uk/projects/trim_galore/), FastQC (http://www.bioinformatics.babraham.ac.uk/projects/fastqc/), TopHat v2.1.1 (Kim et al., 2013), Cufflinks v2.1.1, Cuffdiff, and the makeUCSCfile program on the HOMER software package (http://homer.ucsd.edu/homer/) were used for RNA-seq analysis.

Gene ontology (GO) analysis was performed using Metascape (http://metascape.org/).